Materials & Design 217 (2022) 110592

Contents lists available at ScienceDirect

Materials & Design

journal homepage: www.elsevier.com/locate/matdes

New phase-field model for polycrystalline systems with anisotropic grain boundary properties

Nele Moelans

KU Leuven, Department of Materials Engineering, Kasteelpark Arenberg 44, bus 24.50, 3001 Leuven, Belgium

HIGHLIGHTS

- Phase-field model with inclination and misorientation dependent boundary properties.
- Heterogeneity in grain boundary energy introduced through cross terms in free energy.
- Spurious effects avoided for any set of grain boundary properties.
- Accurately reproduced triple junction angles, also for strong inclination dependence.

GRAPHICAL ABSTRACT

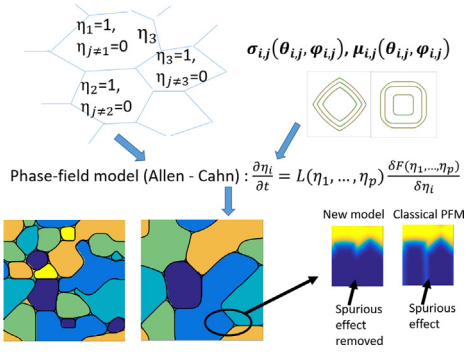

ARTICLE INFO

Article history:
Received 24 January 2022
Revised 16 March 2022
Accepted 22 March 2022
Available online 30 March 2022

Keywords:
Grain growth
Anisotropy
Phase-field model
Facets
Triple junctions

ABSTRACT

In this paper, a new methodology is presented to inlude anisotropic grain boundary properties in a phase-field model. The new approach is thermodynamically consistent and gives accurate control of the inclination and misorientation of grain boundary properties. It is verified that accurate triple junction angles are obtained without ad hoc correction terms and under all conditions, including triple junction angles reaching the extreme values 0° and 180°. Grain boundary wetting is also reproduced. The new model allows us to consider polycrystalline microstructures with very complex grain boundary properties. Simulations show that grain boundary anisotropy may lead to a huge range of effects on the grain structure.

© 2022 The Author(s). Published by Elsevier Ltd. This is an open access article under the CC BY-NC-ND license (http://creativecommons.org/licenses/by-nc-nd/4.0/).

1. Introduction

Metallic and ceramic materials show anisotropy in grain boundary and interface properties [1–4], which has an important effect on the microstructure and properties of the material. Anisotropy in interface or grain boundary properties affects, amongst others, the shape of grains [5–8], the grain boundary kinetics [9,10] and grain size distribution of polycrystalline structures [11,12] and even the spatial distribution of different phases and grain orientations [13]. Alternatively, the presence of certain boundaries or boundary orientations may have a beneficial effect on the bulk properties of the material, e.g. certain boundary types are more resistant to hydrogen embrittlement than others [14]. These observations lead to the design of grain boundary engineered materials [15], having a larger amount of the more beneficial boundaries through advanced heat treatments.

Computer simulations are considered as an important tool to enhance our understanding of the effects of grain boundary properties on the evolution of a microstructure and the overall grain boundary network. In addition, microstructure simulations considering the anisotropy with great detail can support the estimation of grain boundary properties using data assimilation, as shown in

E-mail address: nele.moelans@kuleuven.be

https://doi.org/10.1016/j.matdes.2022.110592
0264-1275/© 2022 The Author(s). Published by Elsevier Ltd.
This is an open access article under the CC BY-NC-ND license (http://creativecommons.org/licenses/by-nc-nd/4.0/).

[16,17], although in these works only misorientation dependence of the grain boundary properties could be considered.

Various approaches have been proposed to include misorientation and, sometimes, inclination dependence in microstructure simulation models, such as multi-phase-field [18,12,19–25], orientation field (or KWC) [26–28], Monte Carlo Potts [29,30] and the level-set [31–33] models. In view of extending the method towards growth and coarsening in multi-component and multi-phase systems, a multi-phase-field model may have several advantages, because of its thermodynamic origin and the natural coupling with CALPHAD Gibbs energies for the bulk phases.

In earlier papers [24,23], the author presented a multi-phase-field model for grain growth simulations in systems with inhomogeneous grain boundary properties and derived quantitative relations between the model parameters and the physical grain boundary energy and mobility of the boundaries. With the introduction of an appropriate tilting function, the model was also extended to multi-component and multi-phase systems [34], and to include grain boundary diffusion [35], leading to wide application of the model formulation, e.g. [13,16,35–45]. It has been implemented in the MOOSE development software [46]. Sparse-data structure based algorithms of the model for large numbers of grains have also been proposed [36,47]. However, in later studies [48], it was observed that triple junction angles deviating largely from 120°, hence with a large difference in the grain boundary or interface energy values, could not be reproduced accurately with this model. In some cases, even qualitatively unphysical behavior of the triple junction was observed. Furthermore, the proposed approach to include inclination dependence in grain boundary energy is too complex for cases with intermediate to strong anisotropy.

Other multi-phase-field models need *ad hoc* correction terms to avoid spurious effects at diffuse interfaces when including anistropy [18,20,49]. To the best of the authors knowledge, a phase-field model that can handle arbitrary anisotropy, is thermodynamically consistent and free of *ad hoc* correction terms or spurious effects, is still lacking. To fill this knowledge gap, a new model solving the existing artefacts is presented here. It will be shown that the unphysical triple junction behavior can be removed and the accuracy with which triple junction angles are reproduced can be drastically improved, simply by adopting a different interpretation of the model parameters for the misorientation dependence in the earlier model [23,24]. Moreover, a new approach to include inclination dependence in a straightforward way is presented. This study shows that the applicability and accuracy of phase-field models for systems with strong anisotropy can be largely increased with the newly proposed methodology.

In the remainder of the paper, first, a summary of the original [23,24] model formulation and parameter relations is given and the observed artefacts are illustrated. Then, the necessary model modifications are discussed and a new procedure to relate the model parameters to the pysical grain boundary properties is presented. The merits of the new parameter choice are illustrated by means of numerical simulations. In this first part, only misorientation dependence of the grain boundary properties is considered. Next, three different ways to include inclination dependence in the improved model are discussed. Their performance and reliability is tested and compared by means of numerical simulations considering a single grain in a matrix, triple junction morphologies and simplified polycrystals with 6 different grain orientations.

2. The original model

In the phase-field model for grain growth as originally presented in [24,23], orientation space is discretized and the different discrete grain orientations are represented using a large set of non-conserved field variables, or phase-fields

$$\eta_1(\mathbf{r},t), \eta_2(\mathbf{r},t), \eta_3(\mathbf{r},t), \ldots, \eta_i(\mathbf{r},t), \ldots \eta_p(\mathbf{r},t).$$

Within each grain, one of the phase-fields, the one representing the particular grain orientation, equals one, while the other phase-fields are equal to zero, see Fig. 1 for an illustration. Grain orientation is assumed to be constant within a grain, although it is possible to consider subboundaries with low misorientation [48,44,13]. At the grain boundaries, the 2 phase-field variables representing the adjacent grains vary smoothly between the values zero and one within a relatively thin diffuse interface region, as shown in Fig. 2. For numerical reasons, the width of this diffuse region, $\ell_{i,j}$, is defined based on the steepest gradient to the phase-field variables within this region, namely as

$$\ell_{i,j} = \frac{1}{|(\mathrm{d}\eta_i/\mathrm{dx})_{x=0}|} = \frac{1}{|(\mathrm{d}\eta_j/\mathrm{dx})_{x=0}|}. \tag{1}$$

This concept is also illustrated in Fig. 2.

The evolution equations of the phase-field variables are derived starting from the time-dependent Ginzburg–Landau equation

$$\frac{\partial \eta_i(\mathbf{r},t)}{\partial t} = -L(\eta_1,\eta_2,\ldots,\eta_p)\frac{\delta F(\eta_1,\eta_2,\ldots,\eta_p)}{\delta \eta_i(\mathbf{r},t)} \tag{2}$$

for all $i = 1 \ldots p$ phase-field variables. The kinetic coefficient L is formulated as a function of the phase-fields as

$$L(\eta_1,\eta_2,\ldots,\eta_p) = \frac{\sum_{i=1}^{p}\sum_{j>i}^{p} L_{i,j}(\phi_{i,j})\eta_i^2\eta_j^2}{\sum_{i=1}^{p}\sum_{j>i}^{p}\eta_i^2\eta_j^2}. \tag{3}$$

where the parameters $L_{i,j}$ are related to the mobility of the grain boundary between a grain with orientation i and one with orientation j, see Fig. 1. Misorientation dependence can thus be introduced taking different values for the $L_{i,j}$. To include inclination dependence of grain boundary mobility, the $L_{i,j}$ can be a function of $\phi_{i,j}$, a normalized vector that specifies the orientation of the normal to the grain boundary between grains with orientations i and j. The direction of the grain boundary normal $\phi_{i,j}$ can be computed from the local gradients of the phase-field variables $\nabla\eta_i$ and $\nabla\eta_j$ as [23,50]

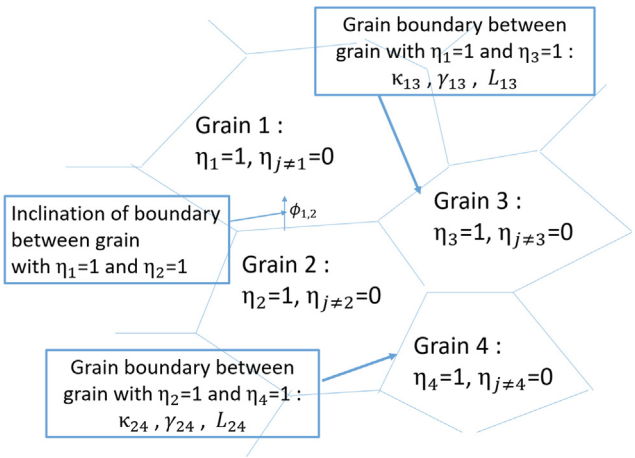

Fig. 1. Graphical illustration of the representation of a grain structure by means of a set of phase-fields η_i, representing the different grain orientations. The properties of a boundary between the grains represented by $\eta_i = 1$ and $\eta_j = 1$ can be manipulated in the model through the model parameters κ_{ij}, γ_{ij} and L_{ij}.

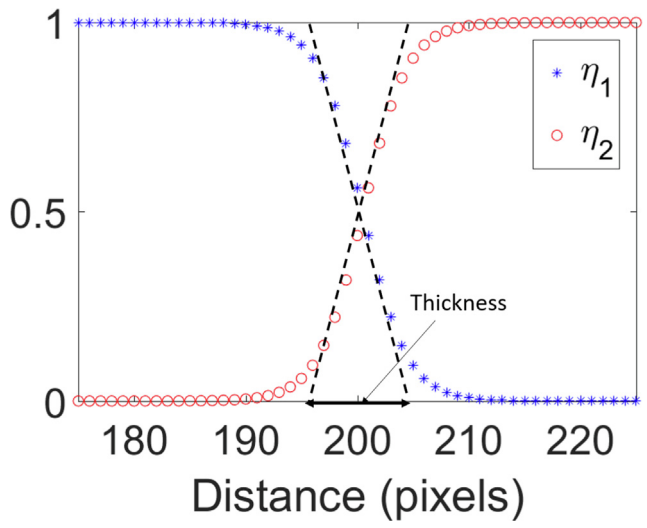

Fig. 2. It is assumed in the model that at a boundary between two grains represented by $\eta_1 = 1$ and $\eta_2 = 1$, the phase-fields η_1 and η_2 change smoothly between 0 and 1 (or 1 and 0) over a finite region, the diffuse interface region, as illustrated in this picture. The meaning of Eq. (1) for the diffuse interface width $\ell_{1,2}$ in the model is graphically illustrated. In the depicted case, the diffuse interface width is 8 pixels.

$$\phi_{i,j} = \frac{\nabla\eta_i - \nabla\eta_j}{|\nabla\eta_i - \nabla\eta_j|}. \tag{4}$$

Since at each boundary only two phase-field variables are assumed to be different from zero, in Eq. (3) only the term $L_{i,j}\eta_i^2\eta_j^2$ remains in the numerator and $\eta_i^2\eta_j^2$ in the nominator when at a boundary between grains i and j, resulting in $L = L_{i,j}(\phi_{i,j})$ at this boundary.

The free energy functional F has the form

$$F = \int_V \left[m f_0(\eta_1, \eta_2, \ldots, \eta_p) + \frac{\kappa(\eta_1,\eta_2,\ldots,\eta_p)}{2} \sum_{i=1}^{p} (\nabla\eta_i)^2 \right] dV, \tag{5}$$

with

$$f_0(\eta_1, \eta_2, \ldots, \eta_p) = \sum_{i=1}^{p} \left(\frac{\eta_i^4}{4} - \frac{\eta_i^2}{2} \right) + \sum_{i=1}^{p} \sum_{j>i}^{p} \gamma_{i,j}(\phi) \eta_i^2 \eta_j^2 + \frac{1}{4}, \tag{6}$$

with $\gamma_{i,j} > 0.5$ and the energy gradient coefficient

$$\kappa(\eta_1, \eta_2, \ldots, \eta_p) = \frac{\sum_{i=1}^{p} \sum_{j>i}^{p} \kappa_{i,j}(\phi_{i,j}) \eta_i^2 \eta_j^2}{\sum_{i=1}^{p} \sum_{j>i}^{p} \eta_i^2 \eta_j^2}. \tag{7}$$

formulated as a function of the phase-field variables and energy gradient coefficients $\kappa_{i,j}$, related to properties of the boundary between grains i and j, using a similar expression as for the kinetic coefficient L.

Irrespective of the model parameter values, f_0 has multiple degenerate minima located at

$$(\eta_1, \eta_2, \ldots, \eta_p) =$$

$$(\pm 1, 0, \ldots, 0), (0, \pm 1, 0, \ldots, 0), \ldots, (0, \ldots, 0, \pm 1)$$

where $f_0 = f_{0,\min} = 0$, corresponding to the different grain orientations. f_0 equals zero within grains and has a positive value at the diffuse grain boundaries contributing to the grain boundary energy.

Depending on the value of $\gamma_{i,j}$, the diffuse profiles of η_i and η_j intersect each other at the middle of the diffuse interface at different values. For $\gamma_{i,j} = 1.5$, the profiles intersect at $\eta_i = \eta_j = 0.5$. For $0.5 < \gamma_{i,j} < 1.5$, they intersect at a value larger than 0.5. For $1.5 < \gamma_{i,j}$, they intersect at a value below 0.5. However, since the phase-fields do not represent phase or grain fractions in this model, the value at which the phase-field profiles intersect has no physical interpretation. Note again that, at a boundary between grains i and j, only the terms in $\eta_i^2\eta_j^2$ in the double summations in Eqs. (6) and (7) differ from zero. The misorientation dependence of the grain boundary energy can therefore be considered within the different $\kappa_{i,j}$ and $\gamma_{i,j}$. The $\gamma_{i,j}$ and $\kappa_{i,j}$ themselves can be a function of the local inclination of the grain boundary $\phi_{i,j}$ given by Eq. (4), when grain boundary energy is inclination dependent. The coefficient m is a constant and affects the grain boundary energy and diffuse interface width of all boundaries.

Combining Eqs. (2) and (5), following evolution equation for the phase-field variables $\eta_i(\mathbf{r}, t)$ was obtained in the absence of inclination dependence

$$\frac{\partial\eta_i(\mathbf{r},t)}{\partial t} = -L(\eta_1, \eta_2, \ldots, \eta_p)\Big[m\left(\eta_i^3 - \eta_i + 2\eta_i \sum_{j\neq i}^{p} \gamma_{i,j}\eta_j^2 \right) - \kappa(\eta_1, \eta_2, \ldots, \eta_p)\nabla^2\eta_i \Big], \tag{8}$$

for $i = 1 \ldots p$. In the presence of inclination dependence, the dependence of the coefficients $\kappa_{i,j}$ and $\gamma_{i,j}$ on the gradients of the phase-fields $\nabla\eta_i(\mathbf{r}, t)$ must be considered as well, resulting in lengthier equations, which are derived in [23]. To obtain the evolution Eq. (8), the η-dependence of $\kappa(\eta_1, \eta_2, \ldots, \eta_p)$ was omitted when taking the derivative $\frac{\delta F(\eta_1,\eta_2,\ldots,\eta_p)}{\delta\eta_i(\mathbf{r},t)}$. This non-variational treatment of the η-dependence of $\kappa(\eta_1, \eta_2, \ldots, \eta_p)$ was needed to avoid the presence of spurious phases at boundaries with a relatively higher energy, as elaborated in [23], Section III.E (i.e. one or several phase-field variables take unintentionally a value different from zero at a diffuse grain boundary region; the so-called *ghost phase* or *'third' phase* contributions at interfaces). This is an important issue of multi-phase-field models which has been discussed several times [18–20,49,51]. These 'third' phase contributions are problematic as they change the interface energy and kinetics and can artificially drag grain boundary movement. Their presence jeoparedizes the possibility to obtain direct relations between the $\kappa_{i,j}, \gamma_{i,j}, L_{i,j}$ and the boundary properties for the individual boundaries. Another way to suppress 'third' phase contributions is by adding higher order terms to the free energy functional; however, so far, there is no unambiguous way to chose the model parameters associated with these higher order terms. Moreover, the higher-order terms are often problematic for the efficiency and numerical stability of the simulations [49].

For each grain boundary, the following relations between its physical grain boundary energy $\sigma_{i,j}$ and mobility $\mu_{i,j}$ and thickness of the diffuse interface $\ell_{i,j}$ (defined according to Eq. (1)), on the one hand, and the model parameters $m, \kappa_{i,j}, \gamma_{i,j}$ and $L_{i,j}$, on the ohter hand, were accordingly obtained using a combined analytical and numerical analysis:

$$\sigma_{i,j} = g(\gamma_{i,j})\sqrt{\kappa_{i,j} m} \tag{9a}$$

$$\ell_{i,j} = \sqrt{\frac{\kappa_{i,j}}{m f_{0,\text{interf}}(\gamma_{i,j})}} \tag{9b}$$

$$\mu_{i,j} = \frac{L_{i,j}\kappa_{i,j}}{\sigma_{i,j}} = \frac{L_{i,j}}{g(\gamma_{i,j})}\sqrt{\frac{\kappa_{i,j}}{m}}. \tag{9c}$$

with i and j refering to the phase-fields representing the two adjacent grains. The values of the functions $g(\gamma_{i,j})$ and $f_{0,\text{interf}}(\gamma_{i,j})$ were evaluated numerically as a function of the value of the model parameter $\gamma_{i,j}$ for $0.5 > \gamma_{i,j} > 40$ and polynomials were fitted to represent the data. A list of the data is given in the supplementary data set http://dx.doi.org/10.17632/87jztf6yt5.1. The polynomial functions and a graph of the data points is shown in the Supplementary Material, section I.

Misorientation dependence in grain boundary energy and mobility is thus introduced in a discrete way through the model parameters $\kappa_{i,j}, \gamma_{i,j}$ and $L_{i,j}$, while for each misorientation, the parameters can be a continuous function of the grain boundary inclination $\phi_{i,j}$. It is shown that, if a sufficient number of discrete grain orientations is included, the model can be considered to be rotationally invariant [52].

With p grain orientations, $t_b = 0.5p(p-1)$ different types of boundaries are considered in the simulation. The phase-field model then contains $3t_b + 1 = 3 \cdot 0.5p(p-1) + 1$ model parameters, namely the $\gamma_{i,j}, \kappa_{i,j}, L_{i,j}$ for the t_b boundaries and m, to fix $3t_b = 3 \cdot 0.5p(p-1)$ grain boundary properties, namely the $\sigma_{i,j}, \ell_{i,j}$ and $\mu_{i,j}$ of the t_b boundary types. The model thus contains sufficient model parameters to specify the diffuse interface width $\ell_{i,j}$ for numerical convenience for each boundary, independent of the physical grain boundary properties of the boundary itself and the physical properties and width of other boundaries. Therefore, in order to resolve the movement of all boundaries with the same accuracy, it was proposed to take a homogeneous grain boundary width along all boundaries, i.e. to take $\ell_{i,j}(\phi_{i,j}) = \ell_{gb}, \forall i,j$, even when the grain boundary properties vary. For this considered model parameter choice, there is still one degree of freedom, since the number of model parameters equals $3t_b + 1$, while the number of grain boundary characteristics to fix, equals $3t_b$. Various sets of model parameter values can thus represent the same set of physical grain boundary properties while all sets will lead to the same simulation results. It is best to chose a set of parameter values with the $\gamma_{i,j}$ as much as possible around the value 1.5, for which symmetrical phase-field profiles are obtained at the interface [23].

With the proposed model formulation and procedure to determine the model parameters, it is possible to obtain highly accurate grain boundary kinetics and triple junction angles for triple junction angles between approximately 100° and 145° degree (see Table 2 and earlier work [23,44,48]). However, unphysical effects are observed for very large and very small triple junction angles, namely when the ratio of the minimum and maximum grain boundary energy approaches or exceeds 2. Firstly, wetting is not appropriately reproduced with the model, even if $\sigma_{1,2} > \sigma_{1,3} + \sigma_{2,3}$. Secondly, for very high triple junction angles, approaching 180°, the triple junction was found to move in the opposite direction than physically expected. Both effects are illustrated in Fig. 3 in the left column. Case 5 and Case 6 refer to the triple junction Cases listed in tables (1) and (2). The model parameters used in the simulations with the original model are given in the Supplementary Material, Section II. These unphysical effects are most likely devoted to the non-variational treatment of the η-dependence of κ in the evolution equations.

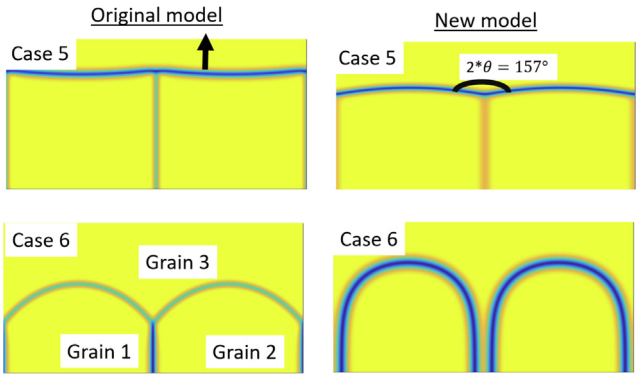

Fig. 3. Left pictures: Unphysical effects at triple junctions observed for the original model formulation (described in Section 2) for large differences in grain boundary energies. For Case 5, a triple junction angle $2\theta = 158°$ is expected. However, this angle cannot be reproduced and, even worse, the triple junction is moving upwards instead of downwards. For Case 6, it is expected that grain 3 wets the boundary between grains 1 and 2. However, the original model cannot reproduce this. The angle remains at 96°. Right pictures: Simulation results obtained with the new model (described in Section 3) considering the same grain boundary energies. This model reproduces well the theoretically expected triple junction behavior. Periodic boundary conditions are taken for the left and right borders and Neumann for the bottom and top borders. See Tables 1 and 2 for the different Cases considered.

3. New approach to treat misorientation dependence of grain boundary properties

Based on the experience with previous models, the prerequisites for the new model formulation are the following.

1. A fully variational derivation of the evolution equations is crucial to reproduce triple junction angle behavior correctly irrespective of the ratios of the grain boundary energies of the joining grain boundaries.
2. Spurious phases at grain boundaries must be avoided irrespective of the ratios of the grain boundary energies, since their presence affects the grain boundary properties and may drag grain boundary migration.
3. To allow for large scale simulations, it must be possible to adapt the length scale of the diffuse grain boundary width independent from the grain boundary energies and mobilities.

The most straightforward solution to avoid the spurious phases, while allowing for a fully variational derivation of the evolution equations, is to take κ constant in the free energy function Eq. (5), i.e. take $\kappa_{i,j} = \kappa, \forall i,j$ in Eq. (7). For $\kappa(\eta_1, \eta_2, \ldots, \eta_p) = \kappa = \text{cte}$, the following evolution equations can be obtained combining (2) and (5), now considering a fully variational approach,

$$\frac{\partial \eta_i(\mathbf{r},t)}{\partial t} = -L(\eta_1, \eta_2, \ldots, \eta_p)\left[m\left(\eta_i^3 - \eta_i + 2\eta_i \sum_{j\neq i}^{p} \gamma_{i,j}\eta_j^2\right) - \kappa\nabla^2\eta_i\right], \tag{10}$$

for $i = 1 \ldots p$.

The misorientation dependence of the grain boundary energy can still be introduced through the model parameters $\gamma_{i,j}$, while the misorientation dependence of the grain boundary mobility is introduced through expression (3) with model parameters $L_{i,j}$. Since they were derived for individual boundaries, the parameter relations Eqs. (9) and polynomial fits for $g(\gamma_{i,j})$ and $f_{0,\text{interf}}(\gamma_{i,j})$, derived for the original model, are still valid, when taking $\kappa_{i,j} = \kappa$ for all boundaries, giving

Table 1
List of combinations of grain boundary energies considered in the triple junction simulations and associated model parameters values as determined with the new procedure to include misorientation dependence. The grain boundary mobility $\mu_{i,j} = 1$ was taken for all boundaries. Note that the grain boundary widths cannot be taken the same for all boundaries. It was taken equal to 1.6 for the boundary with the highest energy, which has the smallest diffuse interface width in this model. For all simulations $\Delta x = 0.2$ was taken and a simulation system of 400×200 pixels.

Case	$\sigma_{1,2}$	$\sigma_{1,3} = \sigma_{2,3}$	κ	m	$\gamma_{1,2}$	$\gamma_{1,3} = \gamma_{2,3}$	$L_{1,2}$	$L_{1,3} = L_{2,3}$	$\ell_{1,2}$	$\ell_{1,3} = \ell_{2,3}$	Δt
equal	0.25	0.25	0.3	0.9375	1.5	1.5	0.833	0.833	1.6	1.6	0.02
1	0.2	0.25	0.3	0.9375	0.9594	1.5	0.6667	0.8333	2.02	1.6	0.02
2	0.25	0.2	0.3	0.9375	1.5	0.9594	0.8333	0.6667	1.6	2.02	0.02
3	0.15	0.25	0.3	0.9375	0.7063	1.5	0.5	0.8333	2.68	1.6	0.02
4	0.25	0.15	0.3	0.9375	1.5	0.7063	0.8333	0.5	1.6	2.68	0.02
5	0.15	0.4	0.36	1.125	0.6328	5.1364	0.4167	1.1111	3.26	1.22	0.02
6	0.4	0.15	0.36	1.125	5.1364	0.6328	1.1111	0.4167	1.22	3.26	0.02
7	0.15	0.75	0.6	1.8750	0.5424	13.7765	0.25	1.25	6.02	1.12	0.005

Table 2
Triple junction angles obtained with the original and new model. Both values are compared with the angle expected from theory. The angles were measured from simulations of the 3-grain structures shown in Supplementary Material, Section VII.

Case	$2\theta_{orig}$	$2\theta_{new}$	$2\theta_{theory}$
equal	118°	118°	120°
1	132°	132°	133°
2	107°	103°	103°
3	150°	144°	145°
4	91°	70°	67°
5	unphysical	157°	158°
6	69°	wetting	wetting
7	unphysical	167°	168°

$$\sigma_{i,j} = g(\gamma_{i,j})\sqrt{\kappa m} \tag{11a}$$

$$\ell_{i,j} = \sqrt{\frac{\kappa}{m}}\sqrt{\frac{1}{f_{0,\text{interf}}(\gamma_{i,j})}} \tag{11b}$$

$$\mu_{i,j} = \frac{L_{i,j}\kappa}{\sigma_{i,j}} = \frac{L_{i,j}}{g(\gamma_{i,j})}\sqrt{\frac{\kappa}{m}}. \tag{11c}$$

This formulation is derived in a fully variational way and guarantees that no 'third' phase contributions will appear at grain boundaries. If a 'third' phase-field would appear, for example the phase-field η_3 at a boundary between two grains represented by the phase-fields η_1 and η_2, this will lead to three positive terms different from zero in the summation with the $\gamma_{i,j}$ in the free energy function f_0 in Eq. (6), compared to only one positive term if only the phase-fields η_1 and η_2 are different from 0 over the diffuse grain boundary region. Furthermore, different from the original approach, the κ-term is now a constant, and the increase of f_0 by the 'third' phase-field cannot be compensated by the lowering effect of the lower values for $\kappa_{1,3}$ and $\kappa_{2,3}$, compared to the value of $\kappa_{1,2}$, on the local value for κ through Eq. (7), as was the case in the original approach. Hence, even if $\gamma_{1,3}$ and $\gamma_{2,3} < \gamma_{1,2}$, it would be energetically unfavorable to have $\eta_3 \neq 0$ and the 'third' phase would disappear at the grain boundary, since the other two phase-fields representing the neigboring grains cannot become equal to 0 within the diffuse interface.

When considering p grain orientations, the new approach contains $2 \cdot 0.5p(p-1)+2$ model parameters, namely $\gamma_{i,j}, L_{i,j}, \kappa$, and m, to fix $3 \cdot 0.5p(p-1)$ grain boundary properties, namely $\sigma_{i,j}, \ell_{i,j}$ and $\mu_{i,j}$. There are thus insufficient model parameters to specify the width of each grain boundary individually; it is therefore no longer possible to have a constant diffuse interface width along all boundaries, as was the case in the original model. In the new model, boundaries with higher energy will have a smaller diffuse interface width than boundaries with lower energy. Still, after fixing the grain boundary energy and mobility of all different types of boundaries (requiring $2 \cdot 0.5p \cdot (p-1)$ model parameters), 2 model parameters remain, which can be used to adjust the overall length scale of the diffuse interface. Although there will be variations in width along the boundaries, the diffuse interface width of all boundaries can still be scaled with a same factor by varying the ratio $\sqrt{\kappa/m}$ for numerical efficiency. In this context, it is important to remember that in the considered phase-field model, the diffuse interface width is purely a numerical parameter. The variations in diffuse interface width in the model do not reflect variations in grain boundary width in the real system.

A procedure to compute all model parameters for a given set of grain boundary energies $\sigma_{i,j}$ and mobilities $\mu_{i,j}$ and a minimum interface width, required for the numerical accuracy $\ell_{\min}$, could be as follows.

1. First consider the boundary with the highest interface energy $\sigma_{i,j} = \sigma_{\max}$. Compute the model parameters for this boundary using parameter relations (11) and taking $\gamma = 1.5$ (or the maximum γ-value $\gamma_{\max}$ to be used in the simulations) and $\ell_{i,j} = \ell_{min} \rightarrow \kappa$ and m to be used for all boundaries and $\gamma_{i,j}$ and $L_{i,j}$ for the boundary with maximum energy are obtained.
2. Then, for all boundaries with energy $\sigma_{i,j}$ and mobility $\mu_{i,j}$ $(i = 1 \ldots p, j = i+1 \ldots p)$
   (a) Compute the model parameters $\gamma_{i,j}$ and $L_{i,j}$ using parameter relations (11) with $\sigma_{i,j}$ and $\mu_{i,j}$ of the boundary and κ and m as computed in step 1.
   (b) Optionally compute the diffuse width $\ell_{i,j}$ using Eq. (11b)

An implementation of this adapted procedure to calculate the model parameters for a given set of grain boundary energies and mobilities is given in the supplementary data set http://dx.doi.org/10.17632/87jztf6yt5.1.

Table 1 gives possible sets of model parameter values considering 8 different combinations of grain boundary energies for triple junction angle simulations. For convenience and generality, non-dimensional values are used in this validation study. It is clear that boundaries with a different energy have a different width in this model, and the boundary with the highest energy has always the smallest width. Note also that, although the grain boundary mobility of all boundaries is taken the same ($\mu_{i,j} = 1$), the values of $L_{i,j}$ for boundaries with a different energy are different. This follows from Eq. (11b), since $g(\gamma_{i,j})$ is different for grain boundaries with a different energy, while the ratio κ/m is the same for all boundaries in this approach.

For the new approach, the simulated triple junction angles are close to the theoretical values (see Supplementary Material, Section VII, for a discussion on how triple junction angles were measured from the simulations). For Case 6, grain 3 wets the boundary between grains 1 and 2 as expected since $\sigma_{1,2} > 2\sigma_{1,3} = 2\sigma_{2,3}$ (see Fig. 3 – Case 6). The boundary between grains 1 and 2 is completely replaced by two boundaries, one between grains 1 and 3 and the other one between grains 2 and 3.

For Cases 5 and 7, with a triple junction angle around and above 160°, the angle is reproduced accurately and the junction is moving in the right direction. Table 2 compares the triple junction angles as obtained with the original and the new approach for equivalent Cases with the theoretical values (the input parameters used for the original approach are given in Supplementary Material, Section II). While both models have a similar accuracy for triple junction angles between 100° and 140°, the new model outperforms the original for very small and very large angles.

4. New approach to include inclination dependence

To illustrate and evaluate the approach, it is assumed that the inclination dependence of the grain boundary energies and mobilities of the different boundaries is known and can be written in the form

$$\sigma_{ij}(\phi_{ij}) = \sigma^0_{ij} f^{\sigma}_{ij}(\phi_{ij}) \tag{12}$$

$$\mu_{ij}(\phi_{ij}) = \mu^0_{ij} f^{\mu}_{ij}(\phi_{ij}) \tag{13}$$

with ϕ_{ij} the inclination, i.e. the unit normal to the grain boundary between the grains represented by η_i and η_j, which can be obtained from the gradients of the phase-field variables $\nabla\eta_i$ and $\nabla\eta_j$ using Eq. (4). Various functional forms have been proposed for f^{σ} and f^{μ}, such as sine or cosine functions [53–55], spherical Gaussian [56] or functions with cusps for facetted growth [57,58]. If only discrete data points are known, as for example extracted from experiments [3,7,59], molecular dynamics simulations [25,60–62] or using a combined experimental-phase-field-simulation approach [16], an inclination dependent function could be fitted through the data points enabling the evaluation of grain boundary stiffness and the Herring relation [6]. It should however be mentioned that, in order to fully consider the 5-dimensional space of grain boundary properties, complicated inclination dependent functions are often needed [4,63,64], or, alternatively, piecewise interpolation through discrete data from a database can be done [25].

Three approaches are evaluated to include the given inclination dependence of the grain boundary energies and mobilities into the new phase-field approach discussed in the previous section (Section 3).

A. The inclination dependence of the grain boundary energy is introduced by multiplying the energy gradient coefficient with an inclination dependent factor, i.e. taking $\kappa(\phi) = \kappa^0 K(\phi)$. This approach is closest to earlier phase-field models considering inclination dependence of interface energy [50,53,54]. The approach is further elaborated in Supplementary Materials, Section III.
B. The inclination dependence of the grain boundary energy is introduced into the phase-field model by means of an inclination dependent multiplication factor $A(\phi)$ in front of the total expression of the heterogeneous energy density. This approach is further elaborated in Supplementary Materials, Section IV. A similar approach has been applied to two-phase and two-grain systems [65].
C. The inclination dependence is introduced through the model parameters γ_{ij}, although in a more rigourous way than proposed in our earlier work [23], while the parameters κ and m remain constant. Approach C is discussed in detail in the next section, since it has not been described before and the numerical simulations show that only approach C can fully avoid the presence of spurious phases at grain boundaries.

An example of the numerical implementation of the three approaches is available in the supplementary data set http://dx.doi.org/10.17632/87jztf6yt5.1.

Alternatively, based on the original Cahn–Hilliard free energy formulation of non-uniform systems [66], for 2-phase materials, inclination dependence of interface energy is often included considering higher order derivatives of the phase-fields in the energy gradient part and considering tensors of energy gradient coefficients [67,68]. However, for multi-phase-field models, such a formulation would most probably lead to 'third' phase contributions and it was therefore not further considered.

5. Inclination dependence through γ_{ij} and L_{ij}

In this approach, the inclination dependence of the grain boundary energies is introduced through the γ_{ij} coefficients in the homogeneous free energy part (6). The coefficients κ and m are kept constant over all boundaries to guarantee that no excessive phase-fields will appear within diffuse regions at grain boundaries. However, due to the non-linear relation between γ_{ij} and the grain boundary energy (see Eq. (9a) and the γ_{ij} dependence of $g(\gamma_{ij})$ given in Supplementary Materials, Section I), it is inappropriate to directly use the inclination dependent factor $f^{\sigma}_{ij}(\phi_{ij})$ in the expression of γ_{ij}. Moreover, from Eq. (9a), it is clear that $g(\gamma_{ij})$ has a linear relationship with the grain boundary energy. Therefore, $g(\gamma_{ij})$ is formulated as function of the inclination dependence of the boundary, using the factor $f^{\sigma}_{ij}(\phi_{ij})$. The inclination dependence of γ_{ij} along the boundary is then implicitly given through the fitted polynomial for $g(\gamma_{ij})$, which gives g^2 as a function of $1/\gamma$ (expression given in Supplementary Materials, Section I).

In this approach, a homogeneous energy density f_0 of the form

$$f_0(\eta_1, \eta_2, \ldots, \eta_p) = \sum_{i=1}^{p}\left(\frac{\eta_i^4}{4} - \frac{\eta_i^2}{2}\right) + \sum_{i=1}^{p}\sum_{j>i}^{p}\gamma_{ij}(\phi)\eta_i^2\eta_j^2 + \frac{1}{4} \tag{14}$$

is used. Given a grain boundary energy of the form (12)

$$g(\gamma_{ij}) = g(\gamma^0_{ij}) f^{\sigma}_{ij} \tag{15}$$

is taken, with γ^0_{ij} determined for $\sigma_{ij} = \sigma^0_{ij}$. The inclination dependence for $\gamma_{ij}(\phi_{ij})$ in the free energy density (14) is then determined through the inverse relation $g^{-1} = \gamma_{ij}$. More concrete, in the simulation program, first the inclination of the grain boundary is computed using Eq. (4). Then, $g_{ij}(\phi_{ij})$ is obtained for the local inclinations ϕ_{ij} from Eq. (15). Next, using the polynomial relation, $1/\gamma_{ij}$ is calculated for the locally obtained values of g^2 and γ_{ij} is finally obtained as the inverse of $1/\gamma_{ij}$.

The evolution equations for the phase-field variables η_i are obtained in a fully variational way starting from Eq. (2) and using Eq. (14) for the homogeneous free energy density in the free energy functional F, giving

$$\begin{aligned}\frac{\partial\eta_i(\mathbf{r},t)}{\partial t} = -L(\eta_1, \eta_2, \ldots, \eta_p)\Big[& m\left(\eta_i^3 - \eta_i + 2\eta_i\sum_{j\neq i}^{p}\gamma_{ij}(\phi_{ij})\eta_j^2\right) \\ & -\kappa\nabla^2\eta_i - m\nabla\cdot\left(\sum_{j\neq i}\left(\frac{\partial\gamma_{ij}}{\partial\nabla\eta_i}\right)\eta_i^2\eta_j^2\right)\Big].\end{aligned} \tag{16}$$

The derivatives of $\gamma_{i,j}$ with respect to $\nabla\eta_i$ can be evaluated indirectly from the inclination dependence of $g(\gamma_{i,j})$ and the polynomial relation between $g(\gamma_{i,j})$ and $\gamma_{i,j}$ using the chain rule (see example Supplementary Materials, section I).

The inlincation dependence of the grain boundary mobility is introduced through the kinetic coefficients $L_{i,j}$ in expression (3), with

$$L_{i,j}(\phi_{i,j}) = L^0_{i,j} f^{\mu}_{i,j}(\phi_{i,j}) f^{\sigma}_{i,j}(\phi_{i,j}). \tag{17}$$

Inspection of Eq. (9c) shows that, due to the presence of $g(\gamma_{i,j})$ in the denominator, it is needed to multiply the $L_{i,j}$ coefficients by $f^{\sigma}_{i,j}$ to obtain the desired inclination dependence for $\mu_{i,j}$.

The following parameter relations are then obtained for this approach

$$\sigma_{i,j}(\phi_{i,j}) = \sigma^0_{i,j} f^{\sigma}_{i,j}(\phi_{i,j}) = g(\gamma^0_{i,j}) f^{\sigma}_{i,j}(\phi_{i,j}) \sqrt{\kappa m} \tag{18a}$$

$$\ell_{i,j}(\phi_{i,j}) = \sqrt{\frac{\kappa}{m}} \sqrt{\frac{1}{f_{0,\text{interf}}(\gamma_{i,j}(\phi_{i,j}))}} \tag{18b}$$

$$\mu_{i,j}(\phi_{i,j}) = \mu^0_{i,j} f^{\mu}_{i,j}(\phi_{i,j}) = \frac{L^0_{i,j}}{g(\gamma^0_{i,j})} \sqrt{\frac{\kappa}{m}} f^{\mu}_{i,j}(\phi_{i,j}), \tag{18c}$$

The diffuse interface width will thus vary along a grain boundary with inclination dependent grain boundary energy, because of the term $f_{0,\text{interf}}(\gamma_{i,j}(\phi_{i,j}))$ in the denominator in Eq. (18b). Parts with a higher energy will have a smaller diffuse interface width. Since the proposed polynomial function was fitted over the range $0.098 < g(\gamma_{i,j}) < 0.766$ ($0.53 \leqslant \gamma \leqslant 40$), it is important to chose a set of model parameters, κ, m and $\gamma^0_{i,j}$, for which $g(\gamma^0_{i,j}) f^{\sigma}(\phi_{i,j})$ remains within this range.

The important advantage of this approach is that a fully variational approach can be applied, while it is guaranteed that spurious phase-field contributions at diffuse boundaries are fully excluded. As explained for the misorientation dependent part, the presence of extra phase-fields at diffuse interfaces will always give rise to extra positive contributions to the summation with $\gamma_{i,j}$ in the energy density and extra gradient contributions, while they cannot lower the values of the prefactors m and κ. If a 'third' phase-field $\eta_3 \neq 0$ at the boundary between grains represented by η_1 and η_2 would obtain a value different from zero, this will result in extra terms in the homogeneous and gradient part of the free energy, always resulting in an increase of the free energy, and hence a driving force to make $\eta_3 = 0$.

6. Numerical simulations with inclination dependence included

The performance in numerical simulations of the three approaches to introduce inclination dependence of the grain boundary energy is here compared for the shrinkage of a single (initially circular) grain within a matrix, the evolution of a 3-grain structure with a single triple junction and the evolution of a limited polycrystalline structure with 6 different grain orientations. Two-dimensional simulations were considered. Then, it is convenient to formulate the inclination dependence of the grain boundary properties as a function of the angle $\phi'_{i,j}$, which is the angle between the x-axis of the system and the normal to the grain boundary $\phi_{i,j}$. $\phi'_{i,j}$ can be computed in the simulations from the gradients of the phase-field variables $\nabla\eta_i$ and $\nabla\eta_j$ as

$$\phi'_{i,j} = \arctan(\phi_{i,j}) = \arctan\left(\frac{\nabla_y\eta_i - \nabla_y\eta_j}{\nabla_x\eta_i - \nabla_x\eta_j}\right), \tag{19}$$

and

$$\begin{aligned} \frac{\partial\phi'_{i,j}}{\partial\nabla\eta_i} &= -\frac{\partial\phi'_{i,j}}{\partial\nabla\eta_j} \\ &= \frac{1}{|\nabla\eta_i - \nabla\eta_j|^2} \begin{bmatrix} -\left(\nabla_y\eta_i - \nabla_y\eta_j\right) \\ \nabla_x\eta_i - \nabla_x\eta_j \end{bmatrix} \end{aligned} \tag{20}$$

6.1. Shrinking grain in matrix

At first, the three models with inclination dependence are applied to simulate the shrinkage of an initially circular grain in a matrix grain. For the case presented here, the following form of the inclination dependence of the grain boundary energy was considered

$$\sigma_{i,j} = \sigma^0_{i,j} f^{\sigma}_{i,j} = \sigma^0_{i,j}\left(1 + \delta_{i,j}\cos\left(4\left(\phi'_{i,j} + \phi^0_{i,j}\right)\right)\right)$$

with $\delta_{i,j} = 0.15, \phi^0_{i,j} = 0$ and $\sigma^0_{i,j} = 0.25$. For this case, the grain boundary mobility is constant, $\mu_{i,j} = 1$ along the boundary. In Supplementary materials, section VIII, several cases, also including cases with inclination dependence in grain boundary mobility, are presented.

The following non-dimensional parameter values were used for this case:

$$\kappa^0 = 0.3,\ \gamma = 1.5,\ m = 0.9375,\ L^0 = 0.833,\ \Delta x = 0.2,$$
$$\Delta t = 0.003.$$

Periodic boundary conditions are applied at the borders of the system. A simulation domain of 100 by 100 pixels is considered, i.e. a size of 20 by 20 (non-dimensional size unit). The simulation is initiated with a circular grain with radius 8 (40 pixels) in the center of the domain. The ratio $\sigma_{\max}/\sigma_{\min} = 1.35$, For inclination dependence model B, the diffuse interface width equals $\ell_{i,j} = 1.6$ along the whole boundary. For inclination dependence model A, the diffuse interface width varies along the boundary as $\ell_{i,j}(\phi_{i,j}) = 1.6 f^{\sigma}_{i,j}(\phi_{i,j})$. For the considered case, this is between $\ell_{\min} = 1.36$ when $\sigma = \sigma_{\min}$ and $\ell_{\max} = 1.84$ when $\sigma = \sigma_{\max}$. For inclination dependence model C, the diffuse interface width varies along the boundary according to Eq. (18b). For this case, this is between $\ell_{\max} = 1.90$ when $\sigma = \sigma_{\min}$ and $\ell_{\min} = 1.40$ when $\sigma = \sigma_{\max}$.

Contour plots at different times in the simulations with the three inclination dependence approaches are depicted in Fig. 4. For all cases, nearly identical results are obtained with the three approaches, regardless of the differences in mathematical formulation and slightly different width of the diffuse interface.

6.2. Triple junctions

Triple junction cases 'equal', 4 and 5 of Table 1 are reconsidered in this section, but including inclination dependence of the grain boundary energies. For each of these three cases, four situations of inclination dependence of the different boundaries are studied. In all situations, a general inclination dependent part of the form

$$f^{\sigma}_{i,j} = 1 + \delta_{i,j}\cos\left(4\left(\phi'_{i,j} + \phi^0_{i,j}\right)\right)$$

is considered for the three boundaries, but with different combinations of values of $\delta_{i,j}$ and $\phi^0_{i,j}$, namely,

g) for all boundaries, $\delta_{i,j} = 0.05$ and $\phi^0_{i,j} = 0$.
h) for all boundaries, $\delta_{i,j} = 0.05$ and $\phi^0_{i,j} = \pi/4$.
i) $\delta_{1,2} = 0, \delta_{1,3} = \delta_{2,3} = 0.15, \phi^0_{1,2} = \phi^0_{2,3} = 0$ and $\phi^0_{1,3} = \pi/4$.

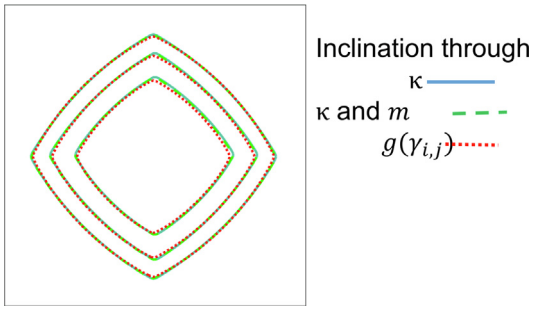

Fig. 4. Simulation results obtained for the shrinkage of a single grain within a matrix assuming the form of inclination dependence of the grain boundary energy as given in the text and using the three different approaches to include the inclination dependence in the phase-field model. Contours (at $\eta_1^2/(\eta_1^2+\eta_2^2)=0.5$) are shown at times 30, 60 and 90.

j) $\delta_{1,2}=\delta_{1,3}=\delta_{2,3}=0.15, \phi^0_{1,2}=0$ and $\phi^0_{1,3}=\phi^0_{2,3}=\pi/4$.

In total, 12 different triple junction systems are thus considered. Each of the 12 systems is simulated using the three models to include inclination dependence. A simulation domain of 100 by 200 pixels is considered, i.e. a size of 20 by 40 (non-dimensional size unit). Periodic boundary conditions are taken for all borders.

Triple junction configurations obtained in the simulations for the 3 cases ('equal', case 4 and case 5) and four situations of inclination dependencies when using the approach with inclination dependence through $\gamma_{i,j}(\phi_{i,j})$ (model C) are presented in Fig. 5. The results obtained using the other two models, namely with inclination dependence through $\kappa=\kappa^0 K(\phi)$ (model A) or through a multiplication factor $A(\phi)$ in front of the free energy expression (model B) are presented in Supplementary Material, Section IX.

The effect of the inclination dependence on the shape of the grains and the triple junction angles is immediately clear. The observed grain shapes can be largely explained refering to the Wulff shape, i.e. the shape corresponding to the lowest total grain boundary energy. Therefore, the boundaries between grains 1 and 3 and grains 2 and 3 have the tendency to be more aligned along 45° for g) and to be closer to horizontal for h). For i), cases 'equal' and 4, a similar effect is observed for the two differently oriented grains. For inclination dependence j), cases 'equal' and 5, the (initially vertically oriented) boundary between grains 1 and 2 becomes serrated, since the vertical direction is 'thermodynamically unstable' for this case. For case 4j), the inclination dependence has made the difference in energy between boundary (1,2) and the other two boundaries so large that grain 3 wets boundary (1,2).

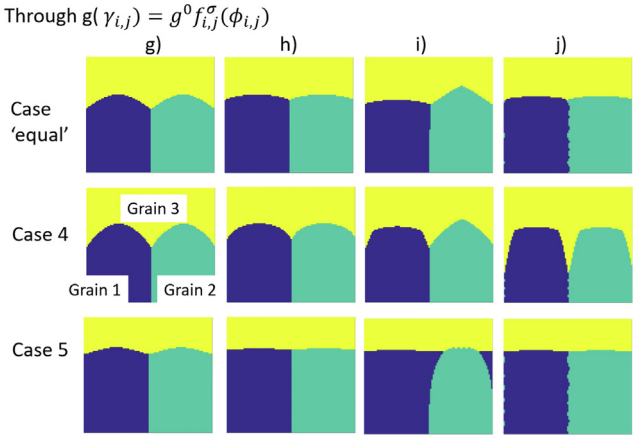

Fig. 5. Overview of the simulated triple junctions obtained for the Cases 'equal', 'sim4' and 'sim5' and inclination dependencies g), h), i) and j), using the approach with inclination dependence through $\gamma_{i,j}(\phi_{i,j})=g^{-1}(\phi_{i,j})$. Only the top 100 rows of pixels of the simulation domain are shown, i.e. the top half.

Moreover, when triple junctions are present, grain shape and evolution are also affected by the mechanical balance between the grain boundary tractions at triple junctions. According to Herring [6,69], the force working on a grain boundary due to curvature is given by

$$P_\kappa=\sigma_{ij}\mathbf{t}+\frac{\partial\sigma_{ij}}{\partial\phi i,j}\mathbf{r}. \tag{21}$$

Mechanical equilibrium in triple junctions then poses the following relation

$$\sum_{i,j}\left(\sigma_{ij}\mathbf{t}+\frac{\partial\sigma_{ij}}{\partial\phi i,j}\mathbf{r}\right)=0, \tag{22}$$

where the summation is taken over the three boundaries that meet in the triple junction. The tangential term drives the grain boundary to move towards its center of curvature to shorten its length. The radial term is a torque that forces the grain boundary to reorient itself towards an orientation with lower energy.

The triple junctions could not be measured accurately enough from the phase-field simulations to quantify the change in triple junction angle due to the inclination dependence of the boundary energy. The phase-field contours are namely smeared out near a triple junction (see the contours near triple junctions in Figs. 6–8). Moreover, the discrete nature of the representation does not allow to locate the triple junction point accurately, while there is substantial change in boundary direction near the triple point, especially when the grain boundary energy has inclination dependence.

Nevertheless, visual inspection indicates that the observed effects of the inclination dependence are very reasonable. Consider, for example, first the simulations with inclination dependence of the form g). For the considered configuration, $\sigma_{1,2}=1.05\sigma^0_{1,2}$, since the boundary between grains 1 and 2 is vertical, i.e. a direction with the highest energy. For this boundary, the normal contribution is 0, i.e. $\partial\sigma_{i,j}/\partial\phi_{i,j}=0$. Furthermore, assuming that boundaries (1,3) and (2,3) have a direction close to the 45°, their energy will be

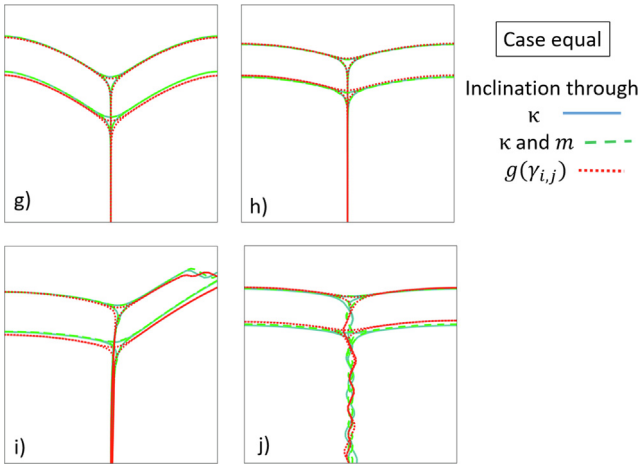

Fig. 6. Contours at $\eta_1^2/(\eta_1^2+\eta_2^2+\eta_3^2)=0.5, \eta_2^2/(\eta_1^2+\eta_2^2+\eta_3^2)=0.5$ and $\eta_3^2/(\eta_1^2+\eta_2^2+\eta_3^2)=0.5$, as obtained from the simulations for Case 'equal' at time 90 for the 4 inclination dependencies g), h), i) and j). The results obtained with the three models to include inclination dependence are superimposed in each figure. Only part of the system, namely 50 by 50 pixels around the triple junction, is shown. For this case, nearly identical results are obtained when using the 3 models to include inclination dependence.

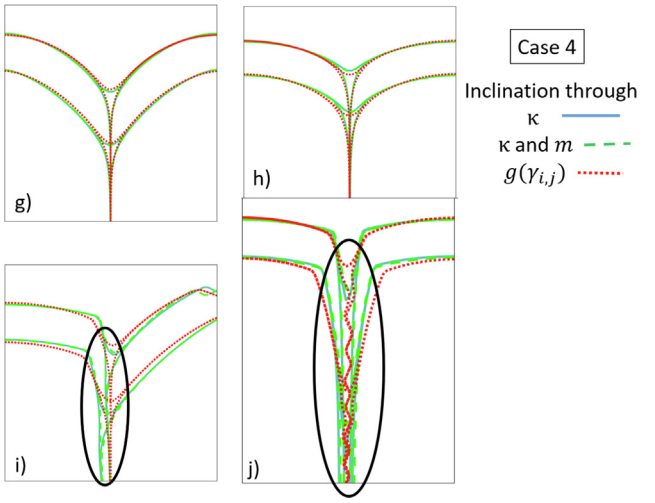

Fig. 7. Contours at $\eta_1^2/(\eta_1^2+\eta_2^2+\eta_3^2)=0.5, \eta_2^2/(\eta_1^2+\eta_2^2+\eta_3^2)=0.5$ and $\eta_3^2/(\eta_1^2+\eta_2^2+\eta_3^2)=0.5$, as obtained from the simulations for Case 4 at time 90 for the 4 inclination dependencies g), h), i) and j). The results obtained with the three approaches to include inclination dependence in the phase-field model are superimposed in each figure. Only part of the system, namely 50 by 50 pixels around the triple junction, is shown (except for j) a slightly higher part is taken to show all essential features). For i) and j), the results obtained with models A and B (through $K(\phi)$ or $A(\phi)$) deviate from those obtained with model C (through $\gamma_{ij}=g^{-1}$ with $g=g^0 f^{\sigma}_{ij}(\phi)$).

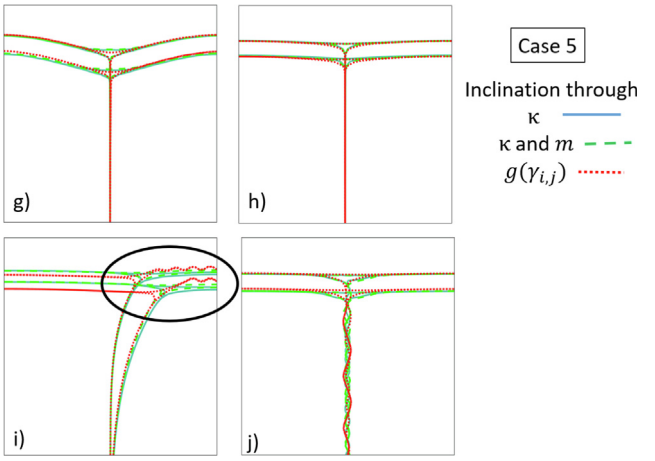

Fig. 8. Contours at $\eta_1^2/(\eta_1^2+\eta_2^2+\eta_3^2)=0.5, \eta_2^2/(\eta_1^2+\eta_2^2+\eta_3^2)=0.5$ and $\eta_3^2/(\eta_1^2+\eta_2^2+\eta_3^2)=0.5$, as obtained from the simulations for Case 5 at time 90 for the 4 inclination dependencies g), h), i) and j). The results obtained with the three approaches to include inclination dependence in the phase-field model are superimposed in each figure. Only part of the system, namely 50 by 50 pixels around the triple junction, is shown. For i) the behavior obtained with the models A and B deviates from that obtained with model C.

close to the minimal energy, meaning $\sigma_{1,3}\approx 0.95\sigma^0_{1,3}$ and $\sigma_{2,3}\approx 0.95\sigma^0_{2,3}$, and the normal component will be small, $\partial\sigma_{i,j}/\partial\phi_{i,j}\approx 0$. Therefore, a smaller triple junction angle is obtained compared to the respective case without inclination dependence. Following a similar reasoning for inclination dependence of the form h), gives that $\sigma_{1,2}=0.95\sigma^0_{1,2}$ and $\partial\sigma_{i,j}/\partial\phi_{i,j}=0$, while boundaries (1,3) and (2,3) cannot be vertical or horizontal in the triple junction, and therefore have a larger value near the triple junction. Consequently, a larger triple junction angle is obtained compared to the case without inclination dependence or with inclination dependence g). For i) and j), the inclination dependence is much stronger and the effects are more pronounced. For i) the boundary between grains 1 and 2 bends, since it is the only boundary for which the grain boundary energy has no inclination dependence, while the other two boundaries have very strong inclination dependence and thus a strong preference for a certain direction. For case 5i), the boundary between grains 2 and 3 will further shorten and finally disappear. For case 4j), the variations in grain boundary energy due to the inclination dependence leads to wetting of the grain boundary between grains 1 and 2 by grain 3, since $\sigma_{1,2}$ along the vertical direction (the direction with highest energy) becomes more than twice as large as $\sigma_{1,3}$ and $\sigma_{2,3}$, for which the boundaries are along a direction of minimal energy.

These twelve simulations illustrate the importance of and enormous variation in effects of inclination dependence of the grain boundary energy on triple junction morphology and migration in polycrystalline structures.

For inclination dependencies g) and h) (the two cases with a mild inclination dependence), the results obtained with the three different approaches to include inclination dependence give nearly identical results. However, for cases i) and j) (the two cases with strong inclination dependence and hence larger variations in grain boundary energy), differences in triple junction morphology were observed when comparing the results obtained with the different models for including inclination dependence.

To further investigate these deviations, in Figs. 6–8, results obtained with the three different approaches to include inclination dependence are superimposed on the same figure for the Cases 'equal', 4 and 5, respectively. The four structures with different inclination dependencies are considered in different subfigures g), h), i) and j). In general, all three approaches give nearly identical results. In the triple junction, the contours obtained with the approach introducing the inclination dependence through $g(\gamma_{ij})$ may deviate slightly from those obtained with the other two approaches (most probably because the difference in γ_{ij}-values makes the phase-field profiles intersect at different values affecting the contour near the triple junction); though, the general behavior and kinetics is the same. However, for Cases 4i) and 4j) and Case 5i), a fundamental difference in behavior is seen when the inclination is introduced through $g(\gamma_{ij})$ (model C) compared to when using the other two approaches (models A and B).

For Case 4i), boundary (1,2) (i.e. the boundary between grains 1 and 2) is curved for models A and B, but remains vertical when inclination dependence is introduced through $g(\gamma_{ij})$ (model C). This difference in behavior is due to the fact that phase-field η_3 obtains values different from zero at the (1,2) boundary for models A and B and not when inclination dependence is introduced through $g(\gamma_{ij})$, as illustrated in Fig. 9. This 'third phase' or 'ghost phase' present at the (1,2) boundary unintentionally affects its properties.

For Cases 4j) and 5i), a similar effect is observed. For Case 4j), the value of η_3 at boundary (1,2) obtains a value different from zero before full wetting of the boundary by grain 3 happens when using models A and B. For inclination dependence model C, η_3, however, does not become different from zero until grain 3 gets the chance to fully wet the boundary and seperate grains 1 and 2. For all three models, grain 3 will finally wet the boundary between grains 1 and 2; however, for models A and B, the wetting occurs much faster. For Case 5i), the phase-field η_1 becomes different from 0 at the boundary between grains 2 and 3 and therefore affects the properties of this boundary, for the results obtained with models A and B. As a result boundary (2,3) is not serrated when using model A or B, while it should remain serrated, which is reproduced only with model C.

These findings illustrate that, especially for large variations in grain boundary energy, one should be cautious for the effects of 'third' phase contributions at diffuse interfaces when using

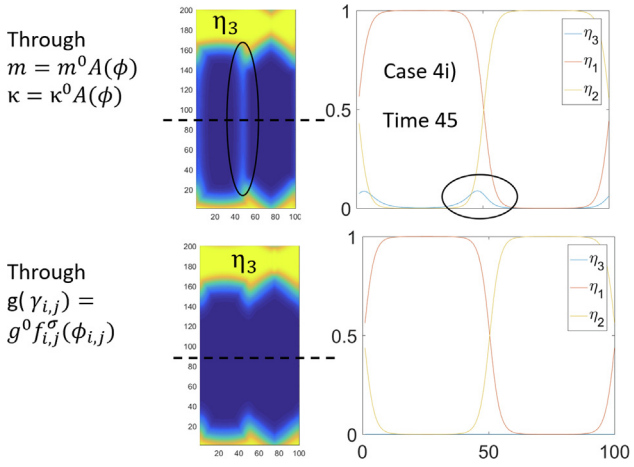

Fig. 9. First row: Illustration of the presence of an undesired 'third' phase contribution from phase-field η_3 at the boundary between the grains represented by phase-fields η_1 and η_2 as obtained for Case 4i) when using inclination dependence models A and B. A colormap of η_3 is given with yellow indicating $\eta_3 = 1$ and blue $\eta_3 = 0$. It is clear that $\eta_3 \neq 0$ at the boundary between grains 1 and 2. The line plot along a horizontal line through the boundary between grains 1 and 2 on the right clearly illustrates the effect: η_3 has an obvious contribution at this boundary. Bottom row: same pictures for the same conditions and at the same time, but obtained using model C, for which inclination dependence of the grain boundary energy is introduced through $g(\gamma_{ij})$. Here $\eta_3 = 0$ at the boundary between grains 1 and 2, as desired. The 'third' phase contribution observed for models A and B affects the behavior of the triple junction angle and of grains 1 and 2 (check the geometry of Case 4i) in Fig. 7).

approaches A and B, while model C guarantees the absence of 'third' phase contributions.

6.3. Polycrystals

Simulations for polycrystalline structures with six different grain orientations were performed using the new model introducing misorientation and inclination dependence of grain boundary energy through the model parameters $\gamma_{i,j}$. The following sets of misorientation and inclination dependencies were considered:

aa) For all boundaries, a common inclination dependence of grain boundary energy is assumed with

$$f^\sigma_{i,j} = 1 + \delta_{ij}\cos(4(\phi'_{i,j} + \pi/4)),$$

with $\delta_{i,j} = 0.15$ and prefactor $\sigma^0 = 0.25$. This corresponds to model parameter values $\kappa = 0.3$, $g^0(\gamma) = \sqrt{2}/3$ $(\gamma^0 = 1.5)$, $m = 0.9375$, $L^0 = 0.833$ for all boundaries. Moreover, $\Delta x = 0.2, \Delta t = 0.003$ and system size is 20×20 (100×100 pixels).

fl) Boundaries between grains with a neighbouring grain orientation (i.e. $|i-j| = 1$ and boundary (1,6)) have a lower overall energy ($\sigma^0 = 0.15$) and an inclination dependence of the grain boundary energy of the form

$$f^\sigma_{ij} = \left(\frac{1}{1+\delta_{ij}}\right)(1+\ \delta_{ij}(|\cos(\phi'_{ij} + \phi^0_{ij})| + |\sin(\phi'_{ij} + \phi^0_{ij})|))$$

with $\delta_{ij} = 1.5$ and $\phi^0_{ij} = n_{ij}\pi/12$ varying with the orientation of the grains, namely $n = 0, 1, 2, 3, 4$ and 5, respectively for the boundaries (1,2), (2,3), (3,4), (4,5), (5,6) and (1,6). For these boundaries, $g^0(\gamma_{ij}) = 0.202$ $(\gamma^0_{ij} = 0.593)$, $L^0_{ij} = 0.3571, \kappa = 0.42$ and $m = 1.3125$ was taken. For the other boundaries, a constant grain boundary energy $\sigma^0 = 0.4$ is assumed, taking, $g^0(\gamma_{ij}) = 0.5387$ $(\gamma^0_{ij} = 2.316)$ and $L^0_{ij} = 0.9524$. Moreover, $\Delta x = 0.2, \Delta t = 0.003$ and system size is 80×80 (400×400 pixels).

gg) For all boundaries, an inclination dependence of the grain boundary energy is considered of the form

$$f^\sigma_{ij} = \left(\frac{1}{1+\delta_{ij}}\right)(1+\ \delta_{ij}(|\cos(\phi'_{ij} + \phi^0_{ij})| + |\sin(\phi'_{ij} + \phi^0_{ij})|))$$

with $\delta_{ij} = 1.5$ and $\phi^0_{ij} = \pi/4$ for $|i-j|$ even and $\phi^0_{ij} = 0$ for $|i-j|$ uneven. A prefactor $\sigma^0 = 0.15$ is taken for boundaries between grains of a neighboring orientation (i.e. $|i-j| = 1$ and boundary (6,1)), while a prefactor $\sigma^0 = 0.25$ is taken for all other boundaries. This corresponds to model parameter values $\kappa = 0.3, m = 0.9375$, $g^0(\gamma_{ij}) = \sqrt{2}/3$ $(\gamma^0_{ij} = 1.5)$ and $L^0_{ij} = 0.833$ for the high energy boundaries and $g^0(\gamma_{ij}) = 0.2828$ $(\gamma^0_{ij} = 0.7063)$ and $L^0_{ij} = 0.5$ for the low energy boundaries. Moreover, $\Delta x = 0.2, \Delta t = 0.003$ and system size is 20×20 (100×100 pixels).

For the three cases, the same constant grain boundary mobility $\mu_{gb} = 1$ was assumed for all boundaries. Simulation results as obtained for these three cases are shown in Fig. 10.

For structure aa), the same energy and inclination dependence is taken for each grain boundary. Given the assumed inclination dependence, it is reasonable to see rather square grains and grain boundaries that are preferentially inclined along the horizontal and vertical direction in the polycrystalline structure. Although this structure is a bit artificial, chosen to test the model capabilities, it could be considered as a simplified representation of a highly textured structure or a ceramic grain structure with strong anisotropy.

For structure fl), the boundaries of neighboring grain orientations have a lower energy and the energy varies with grain boundary inclination, while the other boundaries have higher energy and do not have inclination dependence. The overall structure evolves almost like one would expect for a structure with isotropic properties, since there are only a few boundaries with an inclination dependent grain boundary energy and these boundaries have the lowest energy. Comparison with a simulation of the evolution of the same initial grain structure, but assuming isotropic grain boundary energy $\sigma_{gb} = 0.25$, reveals that boundaries between grains with neigboring orientations have a tendency to lengthen (due to the lower grain boundary energy) and are rather straight

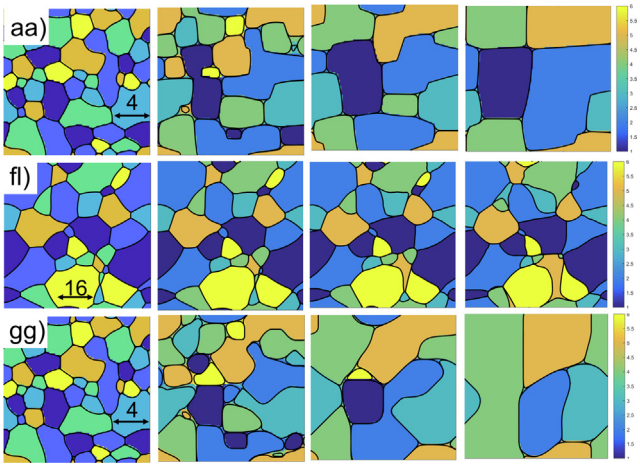

Fig. 10. Time evolution of polycrystalline structures with six different grain orientations and considering orientation and inclination dependent properties as given in the text for cases aa), fl) and gg). For each case, grain structures obtained witht the new model formulation (inclination dependence model C) are shown at dimensionless times 0 (initial), 7.5, 30 and 90. Grains with a different orientation are represented with a different color. Cases aa) and gg) start from the same initial grain structure.

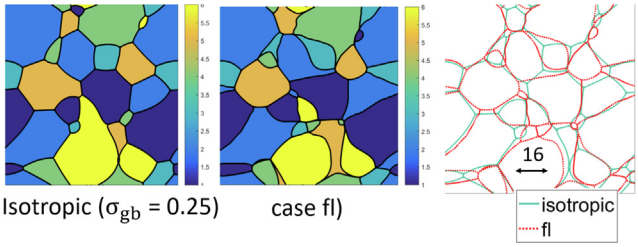

Fig. 11. Left and center figure: Microstructures obtained at time 90, starting from the same initial grain structure, and assuming isotropic grain boundary energy $\sigma_{gb} = 0.25$ and the grain boundary energies of case fl) with inclination dependence and lower energy for boundaries between grains with a neighboring orientation (i.e. $|i-j| = 1$ and boundary (1,6)). Right figure: Grain contours of the two microstructures to show the effects of the inclination dependence in case fl3).

and aligned along a certain direction (due to the inclination dependence of the energy of these boundaries) in structure fl), compared to the isotropic structure (see Fig. 11). Such a structure could be a simplified representation of a grain structure with mostly (high energy) high angle grain boundaries, but with, for low or special misorientation, a low energy for specific inclinations, or for a grain structure containing annealing twins.

For structure gg), all boundaries have the same inclination dependence, but for halve of the boundaries $\phi^0_{ij} = 0$, while for the other boundaries $\phi^0_{ij} = \pi/4$. The effect of this on the polycrystalline structure is clear. Boundaries are rather straight due to the quite strong inclination dependence and have the tendency to be aligned either along the horizontal or vertical direction (boundaries with $\phi^0_{ij} = 0$), or along the diagonal directions (boundaries with $\phi^0_{ij} = \pi/4$). Such a structure could be seen as a simplified representation of a structure with two texture components or prefered grain orientation, and a special or low angle boundary.

In this work, only 2-dimensional simulations of highly simplified grain structures were performed. The collection of microstructures in Fig. 10 illustrates for these systems how important, but also how complex and various, the effect of anisotropy in grain boundary properties on the evolution of a connected grain structure can be. To study the effects of grain boundary anisotropy in a real materials, 3-dimensional simulations have to be performed considering a very high number of grain orientations and using the real anisotropy of the grain boundary properties of the material.

7. Discussion and final conclusions

A largely improved phase-field approach for polycrystalline structures with heterogeneous grain boundary properties is presented and validated. Both the fact that different boundaries can have different energy and mobility and the fact that energy and mobility can depend on boundary inclination are reproduced accurately with the model. Undesired 'third' phase contributions in a phase-field model, even in small amounts, have a tremendous effect on triple junction morphology. In this work, the presence or absence of undesired 'third' phase contributions is analysed for each of the proposed approaches and it is shown that the 'third' phase contributions are completely avoided without a need for ad hoc higher order terms, when all the heterogeneity in grain boundary energy is fully introduced through the model parameters γ_{ij}. The simulations of triple junctions and polycrystalline structures show that the effects of misorientation and inclination dependence of the grain boundary properties can be very important and are highly diverse. Being able to control and predict these effects opens up a huge window for material property optimisation through manipulation of the grain boundary network.

The model is here presented for simulation of curvature driven grain coarsening in single-phase materials. Extension towards multi-phase multi-component systems can be done using the appropriate tilting functions and considering either the bulk Gibbs energies or the grand potentials of the co-existing phases, as presented elsewhere [34,70,71].

Morevoer, various theories suggest that there are several mechanisms for grain boundary migration and that the chosen mechanism may depend on the type of driving force and the grain boundary neighborhood [72–74]. Grain boundary properties can also change due to transitions in the structure of the boundary, the so-called complexion transitions [75]. These are atomistic effects and cannot be predicted by the phase-field model itself. However, if the mechanism and different grain boundary properties under different conditions are known, the proposed model can serve as a framework taking into account these effects accurately to study their effect on the evolution of the microstructure over an extended time.

The model itself and the calculation of the grain boundary normal (Eq. 4) can easily be implemented for 3-dimensional simulations, but one should consider that in 3-dimensions grain boundary properties are a function of 5 parameters (while only a 2 parameters space is required for 2-dimensional simulations) which is more complex to describe and determine.

A strength of the original model was the flexibility of taking the diffuse interface width the same for all boundaries and constant along the boundaries even with variations in grain boundary energy. In the new model, less parameters are available. Although it is still possible to manipulate the overall length scale of the simulations through the ratio κ/m, there are variations in diffuse interface width with variations in grain boundary energy along the boundaries. For the new model, grain boundaries with a lower energy will be wider. The variations in diffuse interface width are somewhat inconvenient from a numerical point of view. On the one hand, a minimum width is required for the thinnest boundaries to resolve the shape and movement of the phase-field variables over the interface; on the other hand, the movement of interfaces may be affected when diffuse profiles of different boundaries overlap, e.g. when the grain size becomes of the same size as the diffuse interface width, which happens earlier for the wider interfaces. But, the presented simulations also show that the effects of variations in diffuse interface width on the overall structure evolution can be kept small by a good choice of the base value for the diffuse interface width ℓ^0_{gb}. Ideally, in the future, a S-PFM grain growth model [76,41], which needs only 2 grid points over a boundary, can be formulated based on the current model.

Data Availability

The simulation scripts, input files and raw data required to reproduce these findings are available to download from Mendeley: "Supporting Material for Improved Quantitative Phase-Field Approach for Simulating Grain Coarsening in Anisotropic Systems with Arbitrary Inclination and Misorientation Dependence", N. Moelans, Mendeley Data, https://doi.org/10.17632/87jztf6yt5.1, 2021.

Declaration of Competing Interest

The authors declare that they have no known competing financial interests or personal relationships that could have appeared to influence the work reported in this paper.

Acknowledgments

The author acknowledges the support of European Research Council (ERC) under the European Union's Horizon 2020 research and innovation program (INTERDIFFUSION, Grant Agreement No. 714754). The computational resources and services used in this work were provided by the VSC (Flemish Supercomputer Center), funded by the Research Foundation - Flanders (FWO) and the Flemish Government - department EWI.

Appendix A. Supplementary material

Supplementary data associated with this article can be found, in the online version, at https://doi.org/10.1016/j.matdes.2022.110592.

References

[1] G. Rohrer, J. Mater. Sci. 46 (2011) 5881.
[2] G. Gottstein, L. Shvindlerman, Grain Boundary Migration in Metals: Thermodynamics, Kinetics, Applications, CRC Press, Taylor & Francis Group, 2010.
[3] J.-E. Brandenburg, L. Barrales-Mora, D. Molodov, G. Gottstein, Scripta Mat. 68 (2013) 980.
[4] V. Bulatov, B. Reed, M. Kumar, Acta Mater. 65 (2014) 161.
[5] W. Rheinheimer, J. Blendell, C. Handwerker, Acta Mater. 191 (2020) 101.
[6] A. Lobkovsky, A. Karma, M. Mendelev, M. Haataja, D. Srolovitz, Acta Mat. 52 (2004) 285.
[7] D. Kirch, E. Jannot, L. Barrales-Mora, D. Molodov, G. Gottstein, Acta Mat. 56 (2008) 4998.
[8] R. Moore, T. Beecroft, S. Rohrer, C. Barr, E. Homer, K. Hattar, F. Boyce, B.L. Abdeljwawad, Acta Mater. 218 (2021) 117220.
[9] A. Bhattacharya, Y.-F. Shen, C.M. Hefferan, S. Li, J. Lind, R. Suter, C. Krill, G. Rohrer, Science 374 (2021) 189.
[10] S. Florez, K. Alvarado, B. Mirgas, N. Bozzolo, D. Chatain, C. Krill, M. Wang, G. Rohrer, M. Bernacki, Acta Mater. 222 (2022) 117459.
[11] A. Kazaryan, Y. Wang, S. Dregia, B. Patton, Acta Mat. 50 (2002) 2491.
[12] E. Shahnooshi, M. Jamshidian, M. Jafari, S. Ziaei-Rad, T. Rabczuk, J. Crystal Growth 518 (2019) 18.
[13] H. Ravash, J. Vleugels, N. Moelans, J. Mater. Sci. 52 (2017) 13852.
[14] H. Mai, X.-Y. Cui, D. Scheiber, L. Romaner, S. Ringer, Mater. Des. 212 (2021) 110283.
[15] V. Randle, Acta Mater. 47 (1999) 4187.
[16] J. Zhang, W. Ludwig, Y. Zhang, H. Henrik, D. Rowenhorst, A. Yamanaka, P. Voorhees, H.F. Poulsen, Acta Mater. 191 (2020) 211.
[17] E. Miyoshi, M. Ohno, Y. Shibuta, A. Yamanaka, T. Takaki, Mater. Des. 210 (2021) 110089.
[18] T. Hirouchi, T. Tsuru, Y. Shibutani, Comput. Mater. Sci. 53 (2012) 474.
[19] H. Salama, J. Kundin, O. Shchyglo, V. Mohles, K. Marquardt, Acta Mater. 188 (2020) 641.
[20] E. Miyoshi, T. Takaki, Comp. Mater. Sci. 112 (2016) 44.
[21] N.C. Admal, J. Segurado, J. Marian, J. Mech. Phys. Solids 128 (2019) 32.
[22] G. Tóth, T. Pusztai, L. Gránásy, Phys. Rev. B 92 (2015) 184105.
[23] N. Moelans, B. Blanpain, P. Wollants, Phys. Rev. B 78 (2008) 024113.
[24] N. Moelans, B. Blanpain, P. Wollants, Phys. Rev. Lett. 101 (2008) 025502.
[25] H.-K. Kim, S.G. Kim, W. Dong, I. Steinbach, B.-J. Lee, Modelling Simul. Mater. Sci. Eng. 22 (2014) 034004.
[26] R. Kobayashi, J. Warren, W. Carter, Physica D 140 (2001) 141.
[27] H. Henry, J. Mellenthin, M. Plapp, Phys. Rev. B 86 (2012) 054117.
[28] B. Korbuly, T. Pusztai, H. Henry, M. Plapp, M. Apel, L. Gránásy, Phys. Rev. E 95 (2017) 053303.
[29] J. Gruber, H. Miller, T. Hoffmann, G. Rohrer, A. Rollett, Acta Mat. 57 (2009) 6102.
[30] J. Allen, C. Cornwell, B. Devine, C. Welch, Comp. Mater. Sci. 71 (2013) 25.
[31] C. Mießen, M. Liesenjohann, L. Barrales-Mora, L. Shvindlerman, G. Gottstein, Acta Mater. 99 (2015) 39.
[32] J. Fausty, N. Bozzolo, D.P. Muñoz, M. Bernacki, Mater. Des. 160 (2018) 578.
[33] H. Hallberg, V. Bulatov, Modell. Simul. Mater. Sci. Eng. 27 (2019) 045002.
[34] N. Moelans, Acta Mater. 59 (2011) 1077.
[35] L. Hou, N. Moelans, J. Derakhshandeh, I.D. Wolf, E. Beyne, Scientific Reports 9 (2019) 1.
[36] M. Tonks, Y. Zhang, X. Bai, P. Millett, Mater. Res. Lett. 2 (2013) 23.
[37] I. Greenquist, M. Tonks, L. Aagesen, Y. Zhang, Comp. Mater. Sci. 172 (2020) 109288.
[38] L. Aagesen, D. Andersson, B.B., et al., J. Nuclear Mater. 541 (2020) 152415.
[39] A. Cheniour, M. Tonks, B.G., et al., J. Nuclear Mater. 532 (2020) 152069.
[40] M. Yang, L. Wang, W. Yan, npj Comput. Mater. 7 (56) (2021).
[41] A. Chadwick, P. Voorhees, Acta Mater. 211 (2021) 116862.
[42] Q. Zhou, B. Xue, S. Gu, Z. Yang, Ceram. Int. 47 (2021) 13783.
[43] X. Zuo, A.M. Bettanini, A. Hilhorst, P. Jacques, N. Moelans, J. Phase Equilibria Diffus. 42 (2021) 794.
[44] M. Tang, B. Reed, M. Kumar, J. Appl. Phys. 112 (2012) 043505.
[45] A. Kunwar, E. Yousefi, X. Zuo, Y. Sun, D. Seveno, M. Guo, N. Moelans, Int. J. Mech. Sci. 215 (2022) 106930.
[46] Moose – grain boundary anisotropy, on-line mooseframework.inl.gov (2020).
[47] L. Vanherpe, N. Moelans, B. Blanpain, S. Vandewalle, Comp. Mater. Sci. 50 (2011) 2221.
[48] N. Moelans, F. Spaepen, P. Wollants, Phil. Mag. 90 (2010) 501.
[49] N. Moelans, F. Wendler, B. Nestler, Comp. Mater. Sci. 46 (2009) 470.
[50] G. McFadden, A. Wheeler, R. Braun, S. Coriel, R. Sekerka, Phys. Rev. E 48 (1993) 2016.
[51] E. Miyoshi, T. Takaki, M. Ohno, Y. Shibuta, ISIJ Int. 60 (2020) 160.
[52] J. Heulens, N. Moelans, Scripta Mat. 62 (2010) 827.
[53] R. Kobayashi, Physica D 63 (1993) 410.
[54] J. Eggleston, G. McFadden, P. Voorhees, Physica D 150 (2001) 91.
[55] A. Karma, D. Tourret, Curr. Opin. Solid State Mater. Sci. 20 (2016) 25.
[56] J. Bair, N. Deshmukh, D. Abrecht, Comput. Mater. Sci. 188 (2021) 110126.
[57] J.-M. Debierre, A. Karma, F. Celestini, R. Guerin, Phys. Rev. E 68 (2003) 041604.
[58] I. Loginova, J.A. Gren, G. Amberg, Acta Mat. 52 (2004) 4055.
[59] X. Liu, D. Choi, H. Beladi, N. Nuhfer, G. Rohrer, K. Barmak, Scripta Mat. 69 (2013) 413.
[60] D. Olmsted, E. Holm, S. Foiles, Acta Mater. 57 (2009) 3704.
[61] K. Janssens, E.H.D. Olmsted, S. Foiles, S. Plimpton, P. Derlet, Nat. Mater. 5 (2006) 124.
[62] C. Hu, Y. Li, Z. Yu, J. Luo, npj Computat. Mater. 159 (2021).
[63] N. Ofori-Opoku, J. Warren, P. Voorhees, Phys. Rev. Mater. 2 (2018) 083404.
[64] B. Runnels, I.J. Beyerlein, S. Conti, M. Ortiz, J. Mech. Phys. Solids 89 (2016) 174.
[65] J. Heulens, B. Blanpain, N. Moelans, Acta Mater. 59 (2011) 2156.
[66] J. Cahn, J. Hilliard, J. Chem. Phys. 28 (1958) 258.
[67] A. Roy, M. Gururajan, Crystal Growth Des. 21 (2021) 1591.
[68] K. Kim, A. Roy, M. Gururajan, C. Wolverton, P. Voorhees, Acta Mat. 140 (2017) 344.
[69] C. Herring, The physics of powder metallurgy, McGraw-Hill, New York, 1949.
[70] S. Chatterjee, N. Moelans, Acta Mater. 206 (2021) 116630.
[71] Y. Coutinho, N. Vervliet, L.D. Lathauwer, N. Moelans, npj Comput. Mater. 6 (2020) 2.
[72] P. Cantwell, M. Tang, S. Dillon, J. Luo, G. Rohrer, M. Harmer, Acta Mater. 62 (2014) 1.
[73] S.L. Thomas, K. Chen, J. Han, et al., Nat Commun 8 (2017) 1764.
[74] E. Homer, S. Foiles, E. Holm, D. Olmsted, Acta Mat. 61 (2013) 1048.
[75] S. Dillon, M. Tang, W. Carter, M. Harmer, Acta Mat. 55 (2007) 6208.
[76] A. Dimokrati, Y.L. Bouar, M. Benyoucef, A. Finel, Acta Mater. 201 (2020) 147.